The Pristine Inner Galaxy Survey (PIGS) I: tracing the kinematics of metal-poor stars in the Galactic bulge

A Arentsen, E Starkenburg, Nicolas F. Martin, V. Hill, R. Ibata, A Kunder, M. Schultheis, K Venn, D Zucker, D Aguado, et al.

Monthly Notices
of the
ROYAL ASTRONOMICAL SOCIETY

MNRAS **491,** L11–L16 (2020)
Advance Access publication 2019 October 18

doi:10.1093/mnrasl/slz156

The Pristine Inner Galaxy Survey (PIGS) I: tracing the kinematics of metal-poor stars in the Galactic bulge

A. Arentsen [1]★ E. Starkenburg,[1] N. F. Martin,[2,3] V. Hill,[4] R. Ibata,[2] A. Kunder,[5] M. Schultheis,[4] K. A. Venn [6] D. B. Zucker,[7] D. Aguado,[8] R. Carlberg,[9] J. I. González Hernández,[10,11] C. Lardo [12] N. Longeard,[2] K. Malhan,[13] J. F. Navarro,[6] R. Sánchez-Janssen [14] F. Sestito,[1,2] G. Thomas,[15] K. Youakim [1] G. F. Lewis [16] J. D. Simpson [17] and Z. Wan [16]

[1]*Leibniz-Institut für Astrophysik Potsdam (AIP), An der Sternwarte 16, D-14482 Potsdam, Germany*
[2]*Observatoire Astronomique de Strasbourg, Université de Strasbourg, CNRS, UMR 7550, F-67000 Strasbourg, France*
[3]*Max-Planck-Institut für Astronomie, Königstuhl 17, D-69117 Heidelberg, Germany*
[4]*Observatoire de la Côte d'Azur, Laboratoire Lagrange, Université Côte d'Azur, CNRS, Blvd de l'Observatoire, F-06304 Nice, France*
[5]*Saint Martin's University, 5000 Abbey Way SE, Lacey, WA 98503, USA*
[6]*Department of Physics and Astronomy, University of Victoria, Victoria, BC V8W 3P2, Canada*
[7]*Department of Physics and Astronomy, Macquarie University, Sydney, NSW 2109, Australia*
[8]*Institute of Astronomy, University of Cambridge, Madingley Road, Cambridge CB3 0HA, UK*
[9]*Department of Astronomy and Astrophysics, University of Toronto, Toronto, ON M5S 3H4, Canada*
[10]*Instituto de Astrofísica de Canarias, Vía Láctea, E-38205 La Laguna, Tenerife, Spain*
[11]*Departamento de Astrofísica, Universidad de La Laguna, E-38206 La Laguna, Tenerife, Spain*
[12]*Laboratoire d'Astrophysique, École Polytechnique Fédérale de Lausanne, Observatoire de Sauverny, CH-1290 Versoix, Switzerland*
[13]*Oskar Klein Centre for Cosmoparticle Physics, Department of Physics, Stockholm University, AlbaNova, SE-10691 Stockholm, Sweden*
[14]*UK Astronomy Technology Centre, Royal Observatory Edinburgh, Blackford Hill, Edinburgh EH9 3HJ, UK*
[15]*NRC Herzberg Astronomy and Astrophysics, 5071 West Saanich Road, Victoria, BC V9E 2E7, Canada*
[16]*Sydney Institute for Astronomy, School of Physics, A28, The University of Sydney, NSW 2006, Australia*
[17]*School of Physics, UNSW, Sydney, NSW 2052, Australia*

Accepted 2019 October 14. Received 2019 October 14; in original form 2019 August 7

ABSTRACT

Our Galaxy is known to contain a central boxy/peanut-shaped bulge, yet the importance of a classical, pressure-supported component within the central part of the Milky Way is still being debated. It should be most visible at low metallicity, a regime that has not yet been studied in detail. Using metallicity-sensitive narrow-band photometry, the Pristine Inner Galaxy Survey (PIGS) has collected a large sample of metal-poor ([Fe/H] < -1.0) stars in the inner Galaxy to address this open question. We use PIGS to trace the metal-poor inner Galaxy kinematics as function of metallicity for the first time. We find that the rotational signal decreases with decreasing [Fe/H] , until it becomes negligible for the most metal-poor stars. Additionally, the velocity dispersion increases with decreasing metallicity for $-3.0 <$ [Fe/H] < -0.5, with a gradient of $-44 \pm 4\,\mathrm{km\ s^{-1}\,dex^{-1}}$. These observations may signal a transition between Galactic components of different metallicities and kinematics, a different mapping on to the boxy/peanut-shaped bulge for former disc stars of different metallicities and/or the secular dynamical and gravitational influence of the bar on the pressure-supported component. Our results provide strong constraints on models that attempt to explain the properties of the inner Galaxy.

Key words: Galaxy: bulge – Galaxy: evolution – Galaxy: formation – Galaxy: halo – Galaxy: kinematics and dynamics – Galaxy: structure.

★ E-mail: aarentsen@aip.de

1 INTRODUCTION

The central few kiloparsecs of the Milky Way are a unique place for Galactic studies as there multiple Galactic components overlap with each other. Most of the mass appears to be in a rotation supported boxy/peanut-shaped bulge that rotates like a solid body, indicative of a bar origin (Howard et al. 2009; Ness et al. 2013b). In recent years, a debate has been ongoing about the importance of an additional classical, pressure-supported component in the bulge (Zoccali et al. 2008; Babusiaux et al. 2010; Kunder et al. 2016). If present, it can only be a small percentage of the mass of the bulge, as constrained by the line-of-sight velocity profiles (Shen et al. 2010; Ness et al. 2013b). However, these profiles are mainly based on metal-rich stars. At lower metallicity, the pressure-supported component may be expected to play a larger role. Additionally, the halo continues down into the central regions of our Galaxy and contributes to the metal-poor inner Galaxy.

Most bulge studies have been based on samples with stars of fairly high metallicity ([Fe/H] >-0.5), since such stars are the most abundant. They already found that sub-solar metallicity stars are more spherically distributed than super-solar metallicity stars (e.g. Zoccali et al. 2017), although they show the same amount of rotation (Ness et al. 2013b). The few studies focusing on metal-poor stars in the inner Galaxy used RR Lyrae stars, a population with mean [Fe/H] $= -1.0$ and age >11 Gyr (Dékány et al. 2013; Kunder et al. 2016). They find that these stars are more spherically distributed than the metal-rich stars and rotate only slightly (if at all). The ARGOS red clump bulge survey contains only 4.4 per cent (522 stars) with [Fe/H] <-1.0 and 0.7 per cent (84 stars) with [Fe/H] <-1.5 (Ness et al. 2013a), not sufficient to study this population in detail.

What is missing from the literature is a comprehensive study of the behaviour of the (very) metal-poor tail of the inner Galaxy. In this Letter, we present for the first time the kinematics as a function of metallicity for a large sample of metal-poor stars (mainly [Fe/H] < -1.0) from the Pristine Inner Galaxy Survey (PIGS, Arentsen et al. in preparation).

2 DATA

Since metal-poor stars in the Galactic bulge are extremely rare, targeted selection is necessary to obtain a large sample of them. PIGS is a sub-survey of the Pristine survey (Starkenburg et al. 2017), which uses a narrow-band *CaHK* filter for MegaCam on the 3.6-m Canada–France–Hawaii Telescope (CFHT) to photometrically search for the most metal-poor stars. The *CaHK* photometry is highly sensitive to metallicity for FGK stars. Candidate metal-poor stars selected from this photometry are followed up using the AAOmega + 2dF multifibre spectrograph on the 3.9-m Anglo-Australian Telescope (AAT) in low/intermediate resolution, which has 400 fibres in a two-degree field of view.

For the selection, we combine our *CaHK* photometry with *Gaia* DR2 broad-band *BP*, *RP,* and *G* photometry (Gaia Collaboration et al. 2016, 2018), or in some later fields with Pan-STARRS1 DR1 *g* and *r* photometry (Chambers et al. 2016). We checked that there are no strong systematic effects between the two selections that affect the results of this Letter. We deredden the photometry using the 3D extinction map of Green et al. (2015, 2018), assuming a distance of 8 kpc. To probe giants in the bulge region, we select stars with $13.5 < G < 16.5$ (*Gaia*) or $14.0 < g < 17.0$ (Pan-STARRS), excluding those that have *Gaia* (parallax − parallax_error) > 0.25 mas to avoid stars closer to us than ∼4 kpc. We do not make any cuts based on the proper motions. The top panel of Fig. 1 shows the location of spectroscopically followed-up metal-poor candidates in a colour–colour diagram. We select stars moving down from the top of the diagram, until there are enough targets to fill all 2dF fibres.

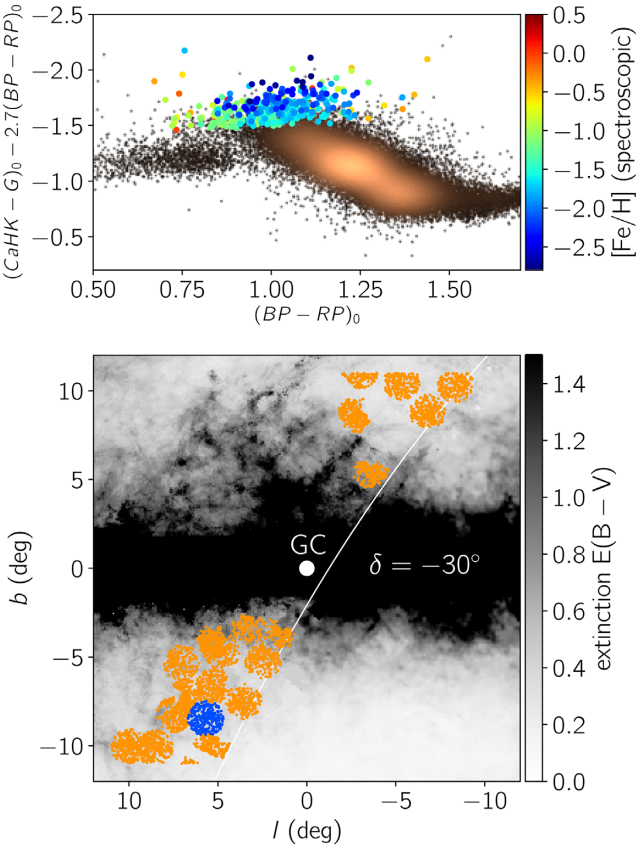

Figure 1. Top: Pristine colour–colour diagram for one field (blue in bottom panel). Metal-poor stars lie towards the top. All stars in this field in our magnitude range that pass the parallax cut are shown (∼ 40 000 stars), of which we observed 350 with the AAT (coloured points). Bottom: coverage of the sample of stars used in this work (after quality cuts). The extinction in the background is a combination of the 3D extinction map from Green et al. (2018) at 8 kpc, available above a declination of −30° (white curve) and reliable at $|b| > 2°$, and the Schlegel, Finkbeiner & Davis (1998) extinction map elsewhere. The colour bar is truncated at $E(B-V) = 1.5$ for clarity.

The spectroscopic observations were performed in 2017 August, 2018 June and August, and 2019 April with the 580V and 1700D gratings. The blue spectra cover a wavelength range of 3800–5800 Å at a resolution R∼1300, the red spectra cover the calcium triplet (CaT) with a wavelength range of 8350–8850 Å at a resolution R∼10 000. Total exposure times were generally 2 h, with sub-exposures of 30 min, to reach a minimum signal-to-noise ratio (S/N) of 20 for the faintest stars. The data were reduced and combined using the AAT `2dfdr` pipeline[1] (v. 6.46) with the standard settings. The spatial coverage of the sample used in this work is shown in the bottom panel of Fig. 1. The PIGS footprint only reaches a declination of −30° since the *CaHK* photometry is obtained from the Northern hemisphere.

[1] https://aat.anu.edu.au/science/software/2dfdr

We used the FXCOR package in IRAF[2] to determine line-of-sight velocities from the CaT spectra. As templates we use synthetic spectra created using the MARCS (Model Atmospheres in Radiative and Convective Scheme) stellar atmospheres and the Turbospectrum spectral synthesis code (Alvarez & Plez 1998; Gustafsson et al. 2008; Plez 2008). We first derive velocities using a fixed template, then derive stellar parameters with the zero-shifted spectra, and finally rederive velocities using templates with stellar parameters close to those of each star, in the following grid: $T_{\rm eff}$ = [5000, 5500] K, $\log g$ = 2.5, and [Fe/H] = [0.0, −1.0, −2.0, −3.0]. Uncertainties are of order 2 km s^{-1}, combining the formal FXCOR uncertainties with an estimate of the systematic uncertainties derived from repeated observations. Stars with large line-of-sight velocity uncertainties ($\varepsilon_{\rm FXCOR} > 5$ km s^{-1}) and double-lined spectra are discarded from our sample. The line-of-sight velocity converted to the Galactic standard of rest $v_{\rm gsr}$ is determined using ASTROPY (v3.0, Astropy Collaboration et al. 2013; Price-Whelan et al. 2018), assuming the peculiar velocity of the Sun from Schönrich, Binney & Dehnen (2010) and circular velocity at the solar radius from Bovy (2015).

To determine stellar parameters $T_{\rm eff}$, $\log g$, and [Fe/H] from the blue spectra, we use the full-spectrum fitting University of Lyon Spectroscopic Software (ULySS, Koleva et al. 2009). We use the well-tested model interpolator created from the empirical MILES library (Prugniel, Vauglin & Koleva 2011; Sharma, Prugniel & Singh 2016), which has for example been used to determine stellar parameters for the X-shooter Spectral Library (Arentsen et al. 2019). This interpolator is calibrated down to [Fe/H] = −2.8, which is perfect for the sample in this work. For more details on the stellar parameter determination, see Appendix A. Typical uncertainties on $T_{\rm eff}$, $\log g$, and [Fe/H] are 120 K, 0.35 dex and 0.2 dex, respectively.

The $T_{\rm eff}$–$\log g$ diagram of the sample passing our quality criteria is shown in the top panel of Fig. 2. In this Letter, we only consider stars with $1.8 < \log g < 3.2$ (black dotted lines), to constrain the sample to stars likely in the bulge volume. This $\log g$ range is the same as that used in Ness et al. (2013a) for red clump stars. This cut removes a significant number of the (very) metal-poor stars, since many of those have low surface gravities and may be located further into the halo on the far side of the bulge. For a discussion on the distances of our sample stars, see Appendix C. Furthermore, the region where the horizontal branch (HB) stars are located is highlighted in red (see Appendix B for more details on the selection and metallicities of the HB stars).

The metallicity distribution of all stars is shown in the bottom panel of Fig. 2. At the low-[Fe/H] end, there is an excess of stars at the limit of the interpolator; several of these may be even more metal-poor than [Fe/H] = −2.8. There are two peaks in the distribution, which can be attributed to two different types of stars: the HB stars and the normal giants. The more metal-rich peak around [Fe/H] ∼−1.1 is that of the HB stars. Although the exact metallicities for the HB stars are somewhat uncertain, they are clearly distinct from the normal giants. The second peak at [Fe/H] = −1.6 is that of the normal giants in the sample and illustrates the success of PIGS in selecting this rare metal-poor population. The overall shape of the metallicity distribution is the result of our specific photometric selection and does not necessarily represent the metallicity distribution function of the underlying population.

[2]IRAF (Image Reduction and Analysis Facility) is distributed by the National Optical Astronomy Observatories, which are operated by the Association of Universities for Research in Astronomy, Inc., under contract with the National Science Foundation.

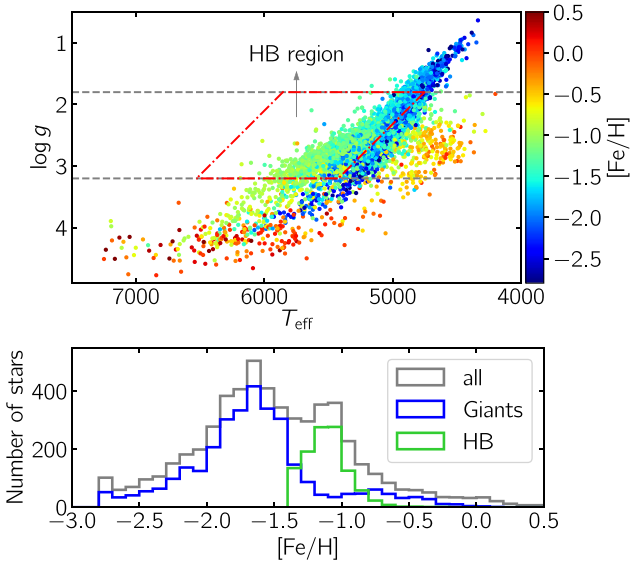

Figure 2. Top: $T_{\rm eff}$–$\log g$ diagram colour-coded by [Fe/H], for the sample making our quality cuts. The $\log g$ cuts are indicated in grey, and the box containing HB stars is shown in red (see Appendix B). Bottom: metallicity distribution of our full sample in grey, with the 4200 stars that have $1.8 < \log g < 3.2$ highlighted in blue (giants) and green (HB stars). The lower [Fe/H] limit of the interpolator is −2.8, causing an apparent excess of stars there.

3 RESULTS

We use our sample to study the kinematics in the inner Galaxy at different metallicities. We investigate the rotation curve and the velocity dispersion as a function of metallicity.

We present the mean line-of-sight velocity as a function of the Galactic longitude in Fig. 3, with the metallicity decreasing from the left- to the right-hand panels. The top row combines all latitudes per longitude bin, the second row shows each AAT field individually, colour-coded by latitude. The dashed lines in these rows are the rotation curves from Shen et al. (2010), who modelled a purely barred bulge which fits the BRAVA data (Howard et al. 2008, 2009). In the bottom row of the figure, we present the corresponding velocity dispersions for both the data and the bar model.

The motions of stars in the most metal-rich bin ($-1.0 <$ [Fe/H] < -0.5) appear quite consistent with the bar models. The more metal-poor stars also show signatures of rotation, but the mean velocity is smaller and decreases with decreasing metallicity until it disappears completely for the most metal-poor stars ([Fe/H] < -2.0).

The rotation of metal-poor stars in the inner Galaxy has previously been seen in the ARGOS data (Ness et al. 2013b), although their sample of metal-poor stars is small and has only one bin ([Fe/H] < -1.0). They find line-of-sight velocities of 20–40 km s^{-1} at $|l| = 10°$, consistent with what we find in our $-1.5 <$ [Fe/H] < -1.0 bin. Additionally, Kunder et al. (2016) showed that the RR Lyrae stars in the inner Galaxy may be rotating slowly, although their sample only contains stars with $|l| < 4°$ so they cannot trace the rotation beyond this. We clearly see for the first time how the rotation changes, and then disappears, as a function of metallicity in the metal-poor tail of the inner Galaxy.

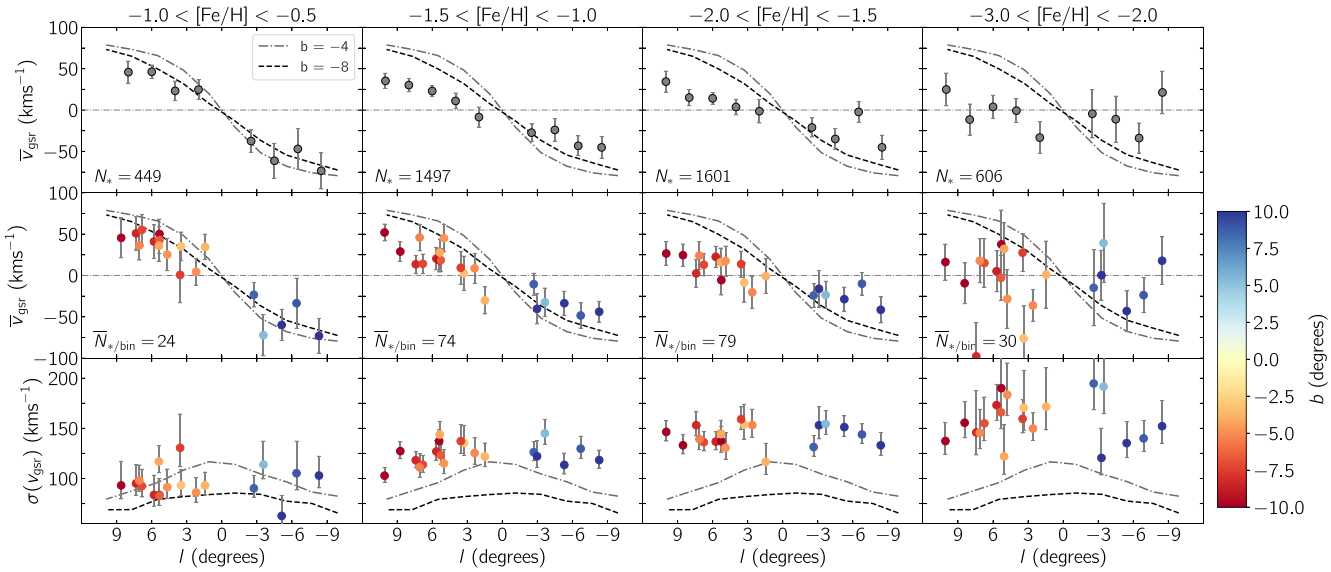

Figure 3. Top row: longitude versus mean line-of-sight velocity in the GSR (v_{gsr}) for different metallicity ranges from left to right (see column title) in bins of 2°. This includes both the normal giants and the HB stars. Lines from the bar model from Shen et al. (2010) have been overplotted. Error bars are $\sigma/\sqrt{N}$. Middle row: the same, but separately for each AAT field where the colour indicates the latitude. Bottom row: similar, but for the standard deviation of v_{gsr} . In each of the panels, only bins with at least 10 stars are shown. The (asymmetric) error bars are $\sqrt{\sigma^2(N-1)/\chi^2_{\pm}}$, with $\chi_{\pm}$ determined for a 68 per cent confidence interval and $N-1$ degrees of freedom.

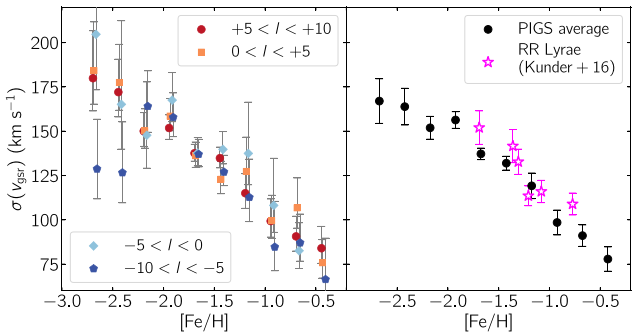

Figure 4. Left: v_{gsr} dispersion as a function of [Fe/H] (bins of 0.25 dex), for four ranges in l. The HB stars are excluded. Different l ranges are offset by 0.01 dex for clarity. Only bins with at least 10 stars are shown. Right: weighted average of the different l ranges, with the bulge RR Lyrae results from Kunder et al. (2016).

Additionally, it is striking how strongly the velocity dispersion increases with decreasing metallicity. The behaviour of the velocity dispersion as a function of [Fe/H] is shown in more detail in Fig. 4. Here we excluded the HB stars, since their metallicity is less well determined. The increase in velocity dispersion with decreasing [Fe/H] appears gradual. The lower dispersions in the range $-10° < l < -5°$ with [Fe/H] < -2.3 could be an indication of substructure, but the sample is small. A linear fit to the average velocity dispersions provides a gradient of -44 ± 4 km s^{-1} dex^{-1}.

Kunder et al. (2016) have previously shown that for inner Galaxy RR Lyrae stars the velocity dispersion increases with decreasing metallicity. Their results have been overplotted in the right-hand panel of Fig. 4 and they generally agree with our findings, although their dispersions appear slightly higher. Ness et al. (2013b) also investigate the velocity dispersion as a function of [Fe/H], with lower [Fe/H] resolution and mainly for higher metallicity stars. For fields with $|l| \leq 10°$ and $b \leq -7.5°$, their relations appear to have similar slopes between $-1.0 <$ [Fe/H] $< +0.5$. Their velocity dispersion at [Fe/H] $= -1.0$ of $\sim$100 km s^{-1} is similar to our findings. Combining the results of PIGS and ARGOS, we find an almost continuous increase in velocity dispersion from [Fe/H] $= +0.5$ down to [Fe/H] $= -3.0$.

4 DISCUSSION

With our large PIGS sample of metal-poor inner Galaxy stars, we can trace for the first time their rotation and velocity dispersion as a function of the metallicity for $-3.0 <$ [Fe/H] < -0.5. We find that the metal-poor stars show a signature of rotation, which decreases in magnitude with decreasing [Fe/H], until it disappears for the most metal-poor stars. The line-of-sight velocity dispersion is continuously increasing with decreasing metallicity. What is the interpretation of the behaviour of these metal-poor inner Galaxy stars? We present a number of possible scenarios.

First, we note that our sample is not completely free of selection effects. Metal-poor stars are generally brighter and thus we may preferentially select stars that are further away at lower metallicity (and therefore less dominated by 'the bulge'). Although we have tried to mitigate this effect through our selection of stars based on surface gravity, a small effect is potentially still present.

If we take our results at face value, a possible explanation is a smooth transition of how much each of the Galactic components (with fixed velocity dispersions) contributes at a certain metallicity. In this case, there is a change from being dominated by a rotation-supported population of a bar or disc at higher metallicities ([Fe/H] > -1.0, Ness et al. 2013b) to being fully dominated by the pressure-supported component like the halo or classical bulge at the lowest metallicities ([Fe/H] < -2.0). Additionally, the stars in our sample are not necessarily confined to the bulge. At the lowest metallicities, the fraction of stars that have large apocentres, and therefore only pass through the bulge, may increase. A transition

between components can naturally explain an increase in velocity dispersion and a decreasing rotational signal with decreasing metallicity. This scenario would also work if the pressure-supported component itself does not rotate at all.

It has been shown that in the solar neighbourhood, the thick disc has a metal-poor tail with [Fe/H] < -1.5 (Kordopatis et al. 2013b), possibly extending all the way down to [Fe/H] < -4.0, (Sestito et al. 2019). If this tail is also present in the inner Galaxy, these stars could contribute to the rotational signal that we see in Fig. 4. Kordopatis et al. (2013b) estimate that in the solar neighbourhood, the fractions of stars with [Fe/H] < -1.5 belonging to the thick disc or the halo are equal (selecting stars with $1 < |Z/\mathrm{kpc}| < 2$ from DR4 of the RAVE survey, Kordopatis et al. 2013a). If we make the simple assumption that this fraction is the same in the inner Galaxy and we combine this with a halo/thick disc mass fraction of 0.10 locally (Kordopatis et al. 2013b) and 0.15 in the inner Galaxy (as derived by Schiavon et al. 2017 based on the Besançon model within a height of 4 kpc and $R_{\mathrm{GC}} = 2$ kpc, from Robin et al. 2012, 2014), we estimate that the halo has ∼1.5 times more stars in this region than the thick disc for [Fe/H] < -1.5. Many assumptions are made here, but this argument shows that at these metallicities the densities of the halo and thick disc only differ by a factor of a few. At higher (lower) [Fe/H] , the thick disc (halo) contribution will dominate over the other.

Alternatively, stars of all [Fe/H] could originate from the disc without an additional halo component, where stars have been mapped into the boxy/peanut bulge in different ways because of their different velocity distributions at the time of the bar formation (e.g. Di Matteo 2016; Debattista et al. 2017). This fits with a continuous increase in velocity dispersion all the way from [Fe/H] $= +0.5$ down to [Fe/H] $= -3.0$ (where this is almost like an age-[Fe/H] relation).

Additionally, a present pressure-supported component can itself be rotating. This can be original rotation from the collapse of a slightly rotating cloud for an *in situ* classical bulge/halo, or alternatively stars in the spheroidal component could have been spun up and/or caught by the bar. The strong dynamical and gravitational effects of the bar should secularly affect all populations in the inner Galaxy (Saha, Martinez-Valpuesta & Gerhard 2012; Saha 2015). Recently, Pérez-Villegas, Portail & Gerhard (2017) used *N*-body simulations to study the influence of the bar and boxy/peanut bulge on the central part of the halo. They find that due to angular momentum transfer, an initially non-rotating halo starts rotating with line-of-sight velocity signatures of ∼15–25 km s^{-1} for $|l| > 5^{\circ}$ with a velocity dispersion of ∼120 km s^{-1} . They also find that a small fraction of the stars (∼12 per cent) are moving on bar-following orbits at the end of their simulation. The exact values of these numbers depend on the model details, but it shows that there can be some rotation in the halo component which is (much) slower than that of the bar. In order for this scenario to explain our metallicity-dependent results, the velocity dispersions for more metal-poor stars had to have been already (much) higher to begin with.

To further disentangle this complex region of our Galaxy, and e.g. to distinguish between an accreted and *in situ* pressure-supported component, additional information is needed. Better distances (e.g. using a combination of parallaxes, spectroscopy and photometry with the STARHORSE code, Santiago et al. 2016; Queiroz et al. 2018) are necessary to derive detailed dynamical properties. Additionally, high-resolution spectroscopic follow-up is necessary to get detailed chemistry of stars, which contains important information not present in metallicities and kinematics alone.

ACKNOWLEDGEMENTS

We thank the referee for their helpful comments. We thank Chris Wegg, Tobias Buck, and Jan Rybizki for helpful discussions and suggestions, and we thank Gail Zasowski for suggesting the PIGS acronym. We thank the organisers of the ESO conference 'The Galactic Bulge at the crossroads' in Pucón, Chile, in 2018 December, where the idea of this Letter was conceived.

We thank the Australian Astronomical Observatory, which have made these observations possible. We acknowledge the traditional owners of the land on which the AAT stands, the Gamilaraay people, and pay our respects to elders past and present. Based on data obtained at Siding Spring Observatory (via programs S/2017B/01, A/2018A/01, OPTICON 2018B/029, and OPTICON 2019A/045, PI: A. Arentsen). Based on observations obtained with MegaPrime/MegaCam, a joint project of CFHT and CEA/DAPNIA, at the CFHT which is operated by the National Research Council (NRC) of Canada, the Institut National des Science de l'Univers of the Centre National de la Recherche Scientifique (CNRS) of France, and the University of Hawaii.

AA, ES, and KY gratefully acknowledge funding by the Emmy Noether program from the Deutsche Forschungsgemeinschaft (DFG). NFM, RI, NL, and FS gratefully acknowledge support from the French National Research Agency (ANR) funded project 'Pristine' (ANR-18-CE31-0017) along with funding from CNRS/INSU through the Programme National Galaxies et Cosmologie and through the CNRS grant PICS07708. FS thanks the Initiative dExcellence IdEx from the University of Strasbourg and the Programme Doctoral International PDI for funding his Ph.D. This work has been published under the framework of the IdEx Unistra and benefits from a funding from the state managed by the French National Research Agency as part of the investments for the future program. CL thanks the Swiss National Science Foundation for supporting this research through the Ambizione grant number PZ00P2 168065. DBZ and JDS acknowledge the support of the Australian Research Council through Discovery Project grant DP180101791. JIGH acknowledges financial support from the Spanish Ministry of Science, Innovation and Universities (MICIU) under the 2013 Ramón y Cajal program MICIU RYC-2013-14875, and also from the Spanish ministry project MICIU AYA2017-86389-P. Horizon 2020: This project has received funding from the European Union's Horizon 2020 research and innovation programme under grant agreement no. 730890. This material reflects only the authors views and the Commission is not liable for any use that may be made of the information contained therein.

The authors thank the International Space Science Institute, Bern, Switzerland for providing financial support and meeting facilities to the international team 'Pristine'.

This work has made use of data from the European Space Agency (ESA) mission *Gaia* (https://www.cosmos.esa.int/gaia), processed by the *Gaia* Data Processing and Analysis Consortium (DPAC, https://www.cosmos.esa.int/web/gaia/dpac/consortium). Funding for the DPAC has been provided by national institutions, in particular the institutions participating in the Gaia Multilateral Agreement.

The Pan-STARRS1 Surveys (PS1) and the PS1 public science archive have been made possible through contributions by the Institute for Astronomy, the University of Hawaii, the Pan-STARRS Project Office, the Max-Planck Society and its participating institutes, the Max Planck Institute for Astronomy, Heidelberg and the Max Planck Institute for Extraterrestrial Physics, Garching, The Johns Hopkins University, Durham University, the University of Edinburgh, the Queen's University Belfast, the Harvard-

Smithsonian Center for Astrophysics, the Las Cumbres Observatory Global Telescope Network Incorporated, the National Central University of Taiwan, the Space Telescope Science Institute, the National Aeronautics and Space Administration under grant no. NNX08AR22G issued through the Planetary Science Division of the NASA Science Mission Directorate, the National Science Foundation grant no. AST-1238877, the University of Maryland, Eotvos Lorand University (ELTE), the Los Alamos National Laboratory, and the Gordon and Betty Moore Foundation.

REFERENCES

Alvarez R., Plez B., 1998, A&A, 330, 1109
Arentsen A. et al., 2019, A&A, 627, A138
Astropy Collaboration et al., 2013, A&A, 558, A33
Babusiaux C. et al., 2010, A&A, 519, A77
Bovy J., 2015, ApJS, 216, 29
Chambers K. C. et al., 2016, preprint (arXiv:1612.05560)
Debattista V. P., Ness M., Gonzalez O. A., Freeman K., Zoccali M., Minniti D., 2017, MNRAS, 469, 1587
Dékány I., Minniti D., Catelan M., Zoccali M., Saito R. K., Hempel M., Gonzalez O. A., 2013, ApJ, 776, L19
Di Matteo P., 2016, PASA, 33, e027
Gaia Collaboration et al., 2016, A&A, 595, A1
Gaia Collaboration et al., 2018, A&A, 616, A1
Green G. M. et al., 2015, ApJ, 810, 25
Green G. M. et al., 2018, MNRAS, 478, 651
Gustafsson B. et al., 2008, A&A, 486, 951
Howard C. D. et al., 2008, ApJ, 688, 1060
Howard C. D. et al., 2009, ApJ, 702, L153
Koleva M., Prugniel P., Bouchard A., Wu Y., 2009, A&A, 501, 1269
Kordopatis G. et al., 2013a, AJ, 146, 134
Kordopatis G. et al., 2013b, MNRAS, 436, 3231
Kunder A. et al., 2016, ApJ, 821, L25
Ness M. et al., 2013a, MNRAS, 430, 836
Ness M. et al., 2013b, MNRAS, 432, 2092
Pérez-Villegas A., Portail M., Gerhard O., 2017, MNRAS, 464, L80
Plez B., 2008, Phys. Scr. Vol. T, 133, 014003
Price-Whelan A. M. et al., 2018, AJ, 156, 123
Prugniel P., Vauglin I., Koleva M., 2011, A&A, 531, A165
Queiroz A. B. A. et al., 2018, MNRAS, 476, 2556
Robin A. C., Marshall D. J., Schultheis M., Reylé C., 2012, A&A, 538, A106
Robin A. C., Reylé C., Fliri J., Czekaj M., Robert C. P., Martins A. M. M., 2014, A&A, 569, A13
Saha K., 2015, ApJ, 806, L29
Saha K., Martinez-Valpuesta I., Gerhard O., 2012, MNRAS, 421, 333
Santiago B. X. et al., 2016, A&A, 585, A42
Schiavon R. P. et al., 2017, MNRAS, 465, 501
Schlegel D. J., Finkbeiner D. P., Davis M., 1998, ApJ, 500, 525
Schönrich R., Binney J., Dehnen W., 2010, MNRAS, 403, 1829
Sestito F. et al., 2019, MNRAS, 484, 2166
Sharma K., Prugniel P., Singh H. P., 2016, A&A, 585, A64
Shen J., Rich R. M., Kormendy J., Howard C. D., De Propris R., Kunder A., 2010, ApJ, 720, L72
Starkenburg E. et al., 2017, MNRAS, 471, 2587
Zoccali M. et al., 2008, A&A, 486, 177
Zoccali M. et al., 2017, A&A, 599, A12

SUPPORTING INFORMATION

Supplementary data are available at *MNRASL* online.

Figure S1 Example fits of three spectra at different [Fe/H] and slightly different $\log g$ and $T_{\rm eff}$.
Figure S2 Same as Fig. S1, but for two HB stars, with slightly different temperatures and metallicities.
Figure S3 Selection of HB stars using the distribution of stars with $-1.4 < [{\rm Fe/H}] < -0.5$ in the $T_{\rm eff}$–$\log g$ diagram.
Figure S4 Comparison of the Bailer–Jones and standard candle HB distances.

Please note: Oxford University Press is not responsible for the content or functionality of any supporting materials supplied by the authors. Any queries (other than missing material) should be directed to the corresponding author for the article.

This paper has been typeset from a TEX/LATEX file prepared by the author.